REPORT DOCUMENTATION PAGE

Form Approved

OMB No. 0704-0188

1. AGENCY USE ONLY (Leave Blank)	2. REPORT DATE	3. REPORT TYPE AND DATES COVERED
	September 2003	Final (10/1/01 – 12/31/03)

4. TITLE AND SUBTITLE
Subcritical Detection of Targets Buried Under a Rippled Interface: Calibrated Levels and Effects of Large Roughness

5. FUNDING NUMBERS
N00014-02-1-0008

6. AUTHOR(S)
K.L. Williams, E.I. Thorsos, D. Tang (all at APL, University of Washington)
J.L. Lopes, C.L. Nesbitt, R. Lim (all at Coastal Systems Station, Naval Sea Systems Command, Panama City, FL 32407-7001)

7. PERFORMING ORGANIZATION NAME(S) AND ADDRESS(ES)
Applied Physics Laboratory
University of Washington
1013 NE 40th St.
Seattle, WA 98105-6698

8. PERFORMING ORGANIZATION REPORT NUMBER

9. SPONSORING/MONITORING AGENCY NAME(S) AND ADDRESS(ES)
Office of Naval Research
800 N. Quincy St.
Arlington, VA 22217-5660
Attn: Dr. John D. Lathrop, Code 32CM

11. SUPPLEMENTARY NOTES
Report to be published in the conference proceedings of *"MTS/IEEE Oceans '03,"* San Diego, CA, September 22-26, 2003

12a. DISTRIBUTION/AVAILABILITY STATEMENT
Approved for public release

12b. DISTRIBUTION CODE

13. ABSTRACT (Maximum 200 words)

This paper describes results of an ongoing modeling and measurement effort investigating shallow grazing angle acoustic detection of targets buried in sand. The measurements were performed in a 13.7-m deep, 110-m long, 80-m wide test pool with a 1.5-m layer of sand on the bottom. A silicone-oil-filled target sphere was buried under a rippled surface with contours formed by raking the sand with a machined rake. Broad band (10 to 50 kHz) transducers were placed onto the shaft of a tilting motor, which in turn was attached to an elevated rail that enabled this assembly to be translated horizontally, permitting acquired data to be processed using synthetic aperture sonar (SAS) techniques. Acoustic backscatter data were acquired at subcritical grazing angles for various ripple wavelengths and heights. Also, the backscattered signals from a free-field sphere and the transmitted signals received with a free-field hydrophone were recorded. Measured roughness information was used in scattering models to calculate the backscattered signal levels from the target and bottom. By taking advantage of the backscattered data and the transmitted data, comparisons more stringent than in previous work were made between predicted and measured buried target backscatter levels.

14. SUBJECT TERMS
backscatter, buried target, rippled interface, ripple height inversion, seabed roughness

15. NUMBER OF PAGES
9

16. PRICE CODE

17. SECURITY CLASSIFICATION OF REPORT	18. SECURITY CLASSIFICATION OF THIS PAGE	19. SECURITY CLASSIFICATION OF ABSTRACT	20. LIMITATION OF ABSTRACT
Unclassified	Unclassified	Unclassified	UL

Subcritical Detection of Targets Buried Under a Rippled Interface: Calibrated Levels and Effects of Large Roughness

J. L. Lopes, C. L. Nesbitt, R. Lim
Coastal Systems Station, Code R21
Naval Sea Systems Command
6703 West Highway 98
Panama City, FL 32407-7001

K. L. Williams, E. I. Thorsos, D. Tang
Applied Physics Laboratory
University of Washington
1013 NE 40th St
Seattle, WA 98105-6698

Abstract- **This paper describes recent results from an on-going modeling and measurement effort investigating shallow grazing angle acoustic detection of targets buried in sand. The measurements were performed in a 13.7-m deep, 110-m long, 80-m wide test-pool with a 1.5-m layer of sand on the bottom. A silicone-oil-filled target sphere was buried under a rippled surface with contours formed by scraping the sand with a machined rake. Broad band (10 to 50 kHz) transducers were placed onto the shaft of a tilting motor, which in turn was attached to an elevated rail that enabled this assembly to be translated horizontally, permitting acquired data to be processed using synthetic aperture sonar (SAS) techniques. Acoustic backscatter data were acquired at subcritical grazing angles for various ripple wavelengths and heights. In addition, the backscattered signals from a calibrated free-field sphere and the transmitted signals received with a free-field hydrophone were recorded. For each bottom configuration, the seabed roughness over the buried target was measured to determine the ripple parameters and to estimate the small-scale roughness spectrum. This roughness information is used in scattering models to calculate the backscattered signal levels from the target and bottom. In previous work, measured signal-to-reverberation ratios were found to compare well with model predictions, demonstrating the accuracy of first-order perturbation theory (for the ripple heights used in those experiments) for frequencies up to 30 kHz. By taking advantage of the backscattered data collected using the free-field sphere and of the acquired transmitted data, more stringent comparisons of predicted buried target backscatter levels to measured levels are made here. Results of a second series of measurements using larger ripple heights to investigate the impact of higher-order scattering effects on buried target detection are presented.**

I. INTRODUCTION

Coastal areas present unique challenges to Mine Countermeasure (MCM) operations. Due to the close proximity of the sea surface and sea bottom, wave-induced effects are significant near the sea bottom, and objects such as mines placed on the sea floor may bury. In order to obtain large standoff distances and high area-coverage rates with sonar, buried targets need to be detected at shallow grazing angles. For sand sediments, where the speed of sound is higher than in the water, this implies the need for detection below the critical grazing angle ("subcritical" grazing angle detection).

Physical models, treating sandy sediments as an attenuating fluid with a flat interface, predict little to no acoustic penetration into sand at subcritical grazing angles. However, recent research has demonstrated that a roughened bottom interface will enhance subcritical penetration. A bottom interface with a random roughness will permit limited penetration, but the dominant mechanism for subcritical penetration appears to be due to scattering from ripple on the water-sediment interface.[1] Ripple acts as a diffraction grating that produces a "quasi-coherent" propagating wave in the sediment.

Nth-order perturbation theory predicts that the maximum depression angle (β_n) of the n^{th}-order field propagating in the sediment due to scattering from periodic ripples is given by

$$\cos\beta_n = \frac{C_2}{C_1}\left(\cos\alpha - \frac{n\lambda_1}{\lambda_r}\right). \qquad (1)$$

Here, C_1 is the water sound speed, C_2 is the sediment sound speed, α is the incident grazing angle, λ_1 is the acoustic wavelength in water, and λ_r is the ripple wavelength.

Recently, a controlled measurement was conducted to investigate subcritical detection of targets buried under a rippled interface.[2] In this measurement, a silicone-oil-filled sphere was buried under a sinusoidal shaped interface with a wavelength of 50 cm and a 1.6-cm root-mean-square (RMS) height about the mean. This initial effort demonstrated subcritical detection via ripple scattering. In addition, the measured signal-to-noise ratios (SNR) were compared to predictions of models that use first-order perturbation theory to calculate the bottom reverberation level as well as the penetration into and out of the sediment. These models use the measured roughness spectrum over the buried target. The predicted SNRs compared well with those measured for frequencies up to 30 kHz. However, above 30 kHz, the measured SNR were found to be higher than those predicted by the model suggesting that higher order effects may need to be considered in the modeling.

The objective of this effort is to further investigate the acoustic detection of targets buried under a rippled interface at subcritical grazing angles. Further analysis of previously collected data from 50-cm wavelength ripples that supports

detection via ripple scattering is presented. In addition, calibrated backscatter levels of signal and reverberation corresponding to 75-cm ripple wavelengths and 1.6- to 2.5-cm RMS heights are obtained and processed with synthetic aperture sonar (SAS) techniques. Results are compared to model predictions including first- and second-order effects.

II. MEASUREMENT SETUP

The measurements reported here were conducted in the Coastal Systems Station Facility 383 test-pool between June 2002 and January 2003. This is a fresh-water pool that is 13.7 m deep, 110 m long and 80 m wide with approximately 1.5 m of sand covering the bottom. The basic measurement setup has been previously described and the reader is referred to [2] for most of these details. Below, a few of these details will be reviewed to clarify features relevant to the present measurements.

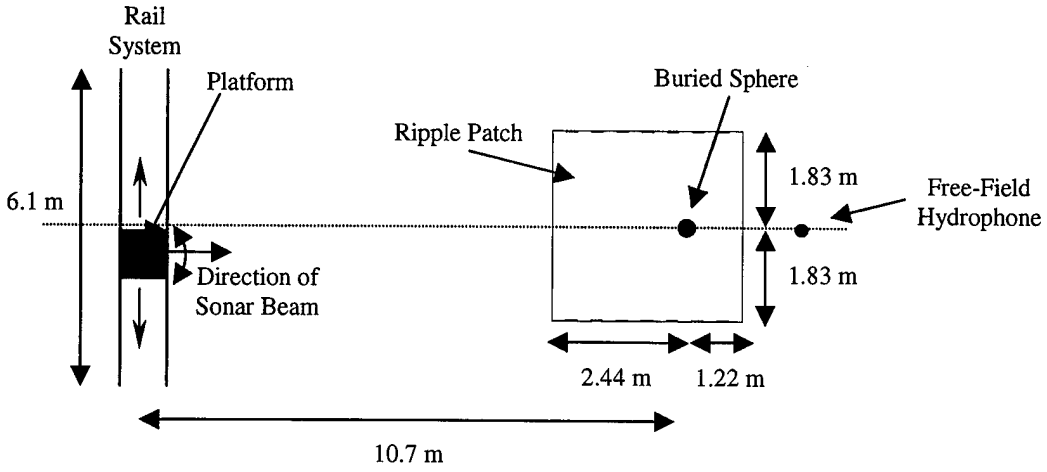

Fig. 1. Target field.

Figure 1 depicts the target field viewed from directly overhead. The target field contained three buried transducers (not shown), a rippled bottom area, one buried target, a rail system with a sonar tower and an extender, two broad-beam, broadband transducers, a free-field sphere (not shown), and a free-field hydrophone. In addition, a sand-scraping apparatus was used to create sinusoidal ripple profiles on the bottom sediment over the buried target, which was a 35.6-cm (14-inch) diameter silicone-oil-filled steel spherical shell. The sinusoidal profile of the scraped bottom patch and the superimposed fine-scale roughness were measured using the In-situ Measurement of Porosity 2 (IMP2) system. (An early version of IMP2 is described in [3].)

Sound speeds in the water column and in the sediment as well as attenuation levels in the sediment were recorded periodically throughout the measurements period. The water column sound speed was measured using a Digibar Model DB-1100 velocimeter. During the initial time frame of the measurement (June through September 2002), the sound speed was found to be 1506 m/s in the top 4 m of the water, and then it varied linearly with depth to a value of 1482 m/s near the water-sediment interface. After this initial time frame, a filtration system was installed in the test pool, and the water column exhibited no velocity gradients for the remainder of the measurement period. The sound speed in the water was measured to be 1498 m/s in October, 1491 m/s in November, and 1463 m/s in December 2002.

The three buried transducers were deployed at various locations in the test pool to determine the longitudinal sound velocity and attenuation in the sediment. These transducers were attached to the legs of a frame that kept the distance between them fixed. One transducer was a Naval Undersea Warfare Center Underwater Sound Reference Detachment (NUWC-USRD) type F42C transducer, and the other two were International Transducer Corporation (ITC) 1089D transducers. The F42C was used as a projector, and the ITC 1089 transducers were used as receivers.

The longitudinal sound speed in the sediment was determined by performing time-of-flight measurements with the buried array. These measurements indicated a sediment sound speed of 1668 m/s when the corresponding water sound speed was 1482 m/s. Using the measured in-water and in-sediment sound velocity, and a porous sediment model[4] for sound propagation in the sediment, the critical grazing angle was calculated to range from 26° to 26.5°.

Figure 2 shows the measured attenuation levels as a function of frequency. These measurements refer to fourteen different data sets that were obtained in five different locations in the test pool. Also plotted on the graph is a line that corresponds to an attenuation level of 0.33 dB/kHz/m, which is a value typical of sands.

As shown in Fig. 1, the rippled bottom area was a patch

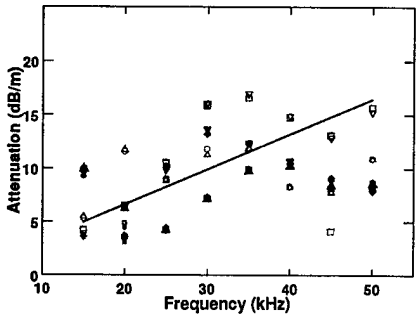

Fig. 2. Attenuation levels versus frequency.

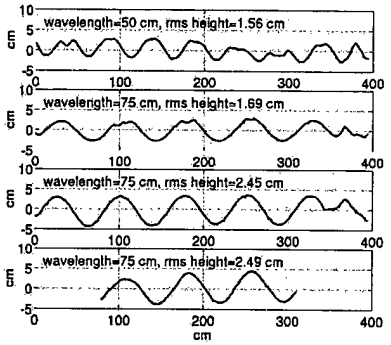

Fig. 3. Measured ripple profiles.

approximately 3.66 m (12 ft) in length by 3.66 m (12 ft) in width, and it started about 8.2 m from the rail system. The sand scraper was used to form four different sinusoidal profiles on this patch. The designed parameters (wavelength and root-mean-square (RMS) height) of these profiles are summarized in Table 1. In addition to these profiles, data were also collected with a flattened bottom, created by divers dragging a weighted bar over the surface of the 3.66-m by 3.66-m bottom patch.

As noted previously, the bottom roughness over the buried target was measured with the IMP2, which was developed primarily for the purpose of measuring fine-scale sediment density variability.[3,5] Here, it provided a useful check of the fidelity of the overall bottom contour after scraping as well as a measure of fine scale roughness parameters. Figure 3 shows four different measurements of the ripple profiles by IMP2. Above the wavenumber associated with each ripple wavelength, a power law was fit to the roughness spectrum to characterize fine scale roughness, resulting in an estimated two-dimensional power-law spectrum for each ripple configuration. Table 1 lists the IMP2 measured ripple wavelength and RMS height for each ripple configuration and the computed spectral exponent, γ_2 ,and spectral strength,[5] w_2, for the fine-scale features superimposed on each ripple configuration.

Despite fairly uniform rakings with the sand scraper, the fine-scale roughness is found to exhibit significant variability. Note that IMP2 measurements performed on the two similarly raked 75-cm wavelength, 2.5-cm (RMS) height ripple profiles exhibit moderate variability in the estimated fine-scale spectral parameters. This variability leads to uncertainty in SNR predictions for the buried sphere and suggests that calibrated target levels would be better for data/model comparisons.

To allow for more robust data calibration, a free-field hydrophone and a free-field sphere were deployed in the target field. The free-field hydrophone was an ITC 1089D transducer, situated approximately 0.6 m above the bottom and about 14 m from the rail system. It was held rigidly in place by a Delrin tube that was in turn attached to a small bottom-mounted tripod. This hydrophone was used to record each transmitted signal as the transducers were translated along the rail system. Thus, it provided knowledge of the transmitted levels and of the locations of the transducers attached to the rail as they moved along the rail.

A 20.32-cm (8-inch) diameter free-field sphere was also utilized in the measurement. Divers deployed this sphere after the buried target data were collected. It was located 3.89 m above the bottom sediment and placed directly over the buried sphere. Backscattered signals from the free-field sphere were used to determine calibrated levels for the SAS processed data.

For each ripple profile, the burial depth of the target relative to the mean sand surface and its horizontal location relative to ripple features were measured (after collection of all acoustic data) by divers with the aid of a reference bar and probe. Table 2 lists the burial depth to the top of the sphere

Table 1. Designed and measured/computed ripple parameters.

Designed		Measured/Computed			
λ_r (cm)	RMS Height (cm)	λ_r (cm)	RMS Height (cm)	γ_2	w_2 ($cm^{(4-\gamma_2)}$)
50	1.8	50	1.6	3.53	$2.79x10^{-4}$
75	1.8	75	1.7	3.76	$5.1x10^{-4}$
75	2.7	75	2.5	2.32	$3.6x10^{-4}$
75	2.7	75	2.5	2.53	$2.63x10^{-4}$

Table 2. Measured burial depth and location of sphere.

λ_r (cm)	RMS Height (cm)	Depth (cm) / Location
50	1.6	5 / Under Crest
75	1.7	5 / Under Crest
75	2.5	8.5 / Under Crest
75	2.5	17 / 10.5 cm on source side of Trough minimum

and the sphere's location for each ripple profile. Depth uncertainties are estimated to be ± 1cm and horizontal uncertainties to be ± 5 cm.

Scattering data from the buried target were obtained by translating the sonar along the rail platform and taking data in approximately 2.5-cm increments. Data were obtained for the various bottom configurations (rippled and flat) for 1.76- and 3.89-m transducer heights above the bottom corresponding to grazing angles of 10° and 20°, respectively, which are both below the critical grazing angle. The free-field sphere data were acquired when the source transducer was 3.89 m above the bottom and directed horizontally. All data were acquired in the frequency range of 10 to 50 kHz.

Transmitted pulses were 0.2-ms sinusoidal signals that had a 0.04-ms taper on the leading and trailing edges to minimize ringing in the waveforms generated by the source. The received signals were amplified and filtered to include frequencies within ±5 kHz of the source center frequency, then digitized at a sample frequency of 1 MHz.

III. RESULTS AND DISCUSSION

A. Data Reduction

The acquired data were processed using a ω-k (wavenumber) algorithm as described by Hawkins.[6] The processed data, which are proportional to voltage, were mapped to the appropriate range and cross-range and used to generate a SAS image. Here range and cross-range are measured parallel and perpendicular to the direction of the acoustic beam, respectively.

The processed data were further analyzed to determine calibrated signal and reverberation backscatter levels. An estimate of the reverberation level was determined by taking an average of the reverberation intensities in a patch 2 m wide in cross-range by 0.5 m long in range in a location near the target. The calibrated backscatter level, EL in dB, was determined using,

$$EL = EL_{SAS} - G_{SAS} - SPL_{INTERFACE} \quad . \qquad (2)$$

Here EL_{SAS} is the backscattered level in dB obtained after SAS processing, G_{SAS} is the gain in dB due to SAS processing, and $SPL_{INTERFACE}$ is the sound pressure level in dB incident on the water-sediment interface directly above the buried sphere. G_{SAS} was obtained using the free-field sphere data by comparing the echo level from a single ping (obtained with the transducers on the rail at the position of closest approach) with the level obtained using the rail system and SAS processing techniques. $SPL_{INTERFACE}$ was obtained by using the level measured with the free-field hydrophone and accounting for the difference in propagation loss to the location directly over the buried sphere.

B. SAS Images

Typical SAS images associated with a range from 8 to 12 m and a 1-m cross-range width are shown in Figs. 4 and 5 for several acoustic frequencies. Figures 4 and 5 correspond to data collected with a 50-cm wavelength sinusoidal ripple and a flat bottom, respectively. In all instances, the grazing angle is 20° over the buried sphere. The color scale of each image in Fig. 4 corresponds to a logarithmic scaling of the backscatter intensity relative to the image maximum over a 15 dB range. To facilitate comparison with Fig. 4, Fig. 5(a) is plotted on the same color scale as Fig. 4(b) and Fig 5(b) is plotted on the same color scale as Fig. 4(d). Between 10.5 m to 11.0 m range, a well-focused acoustic return from this sphere appears in each image in Fig. 4 with a cross-range resolution of about 10 to 13 cm and a range resolution of about 22 cm. On the other hand, the buried sphere was not detected in the images of Fig. 5. This comparison strongly suggests the subcritical detection observed here is caused by ripple scattering.

As further evidence of ripple scattering, note that the location of the maximum level from the buried sphere seen in each image in Fig. 4 exhibits a systematic change in range with changing frequency. For example, the maximum level occurred at a range of about 10.9 m for a frequency of 10 kHz, while it was 10.7 m at 50 kHz. The low frequency (10 kHz) variation is likely a result of systematic measurement error (e.g., reverberant contamination of the target backscatter) but, even with this accounted for, a subtler trend remains over the entire band. A plausible explanation for the subtler trend arises from inspection of Eq. (1), which predicts a change with frequency in the first-order diffracted grazing angle β_1 that illuminates the target. The optimal β_1 ranges from 44° at 10 kHz to 12° at 50 kHz, which corresponds to movement of the patch on the bottom contributing to target illumination over an 80-cm range. This, in turn, impacts the overall two-way time associated with range.

Figure 6 demonstrates this with a plot of the two-way time versus frequency for the peak intensity. Unfilled circles represent times determined from data that may be unreliable. At 10 kHz there is some unavoidable data contamination by echoes from concrete blocks deployed near the test area. The open circle point at 50 kHz has a SNR of less than 15 dB, which could result in a time shift. The filled circles all have SNR greater than 15 dB and are believed to be unaffected by contamination from concrete block echoes. The black line in

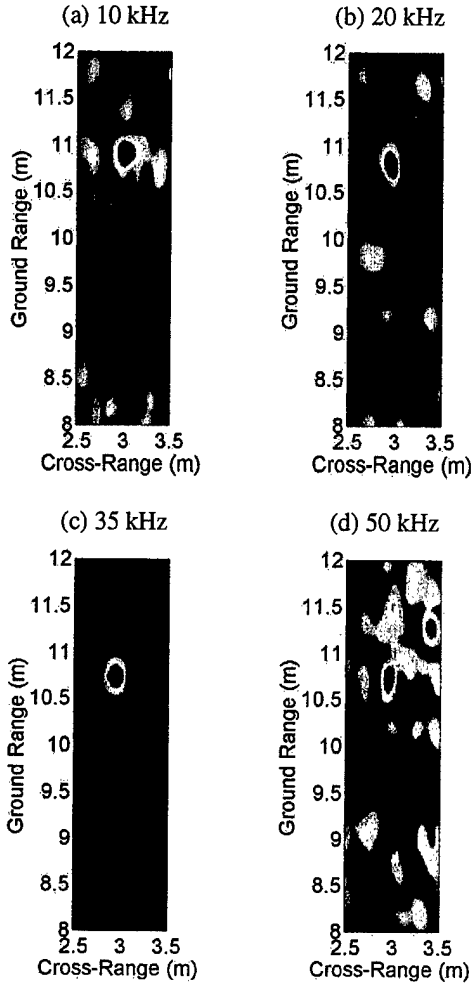

Fig. 4. SAS images for rippled bottom with a 50-cm wavelength.

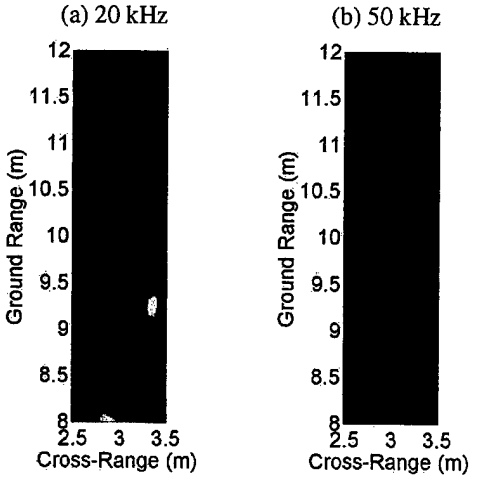

Fig. 5. SAS images for a flattened bottom.

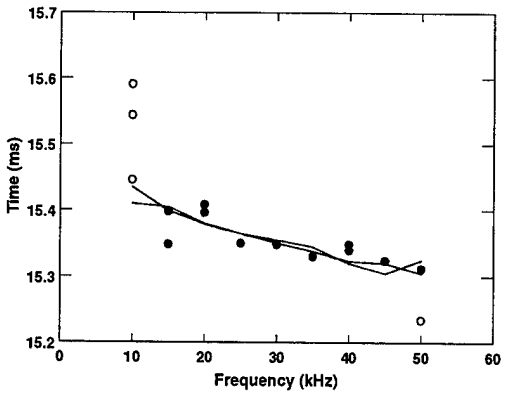

Fig. 6. Two-way time versus frequency.

Fig. 6 represents travel time calculations based on the measurement geometry and Eq. (1) assuming the diffraction is predominantly first order. Furthermore, the red line corresponds to travel times determined from a high-fidelity simulation of the scattering by the buried sphere via transition- (T-) matrix calculations carried out to second order in perturbation theory.

Good agreement between these comparisons is a strong indication that, except at the low frequency end, the observed range shifts are not due to systematic measurement error but are driven by target illumination via ripple scattering. Notably, both the T-matrix and geometry-based predictions yield monotonically decreasing travel times up to about 45 kHz, where the T-matrix prediction then leads to a small but noticeable upward shift of the travel time at 50 kHz. As verified by further T-matrix simulations carried out to only first order in perturbation theory, this is a consequence of second-order diffraction effects becoming important. However, we do not expect this effect to be observable in the data. While travel times can be extracted with high precision from the data (with uncertainty much less than the symbol size in Fig. 6), other effects will likely come into play that could affect the data/model comparison. For example, the model assumes perfectly sinusoidal ripples that are one-dimensional and are not terminated at the edges of the ripple patch. For the measurements with a 50-cm ripple wavelength, the ripple profile had significant deviations from a sinusoid (top profile in Fig. 3). We consider the resultant data variability, as indicated by the spread of the filled circles about the predicted trend lines, to be an appropriate measure of the degree to which the data/model comparison is meaningful. This level of variability could easily hide the predicted second-order trend at the highest frequencies.

C. Calibrated Signal Levels

Calibrated signal levels corresponding to the 75 cm ripple wavelength cases in Table 1 are compared to predictions of three different target scattering models and a reverberation

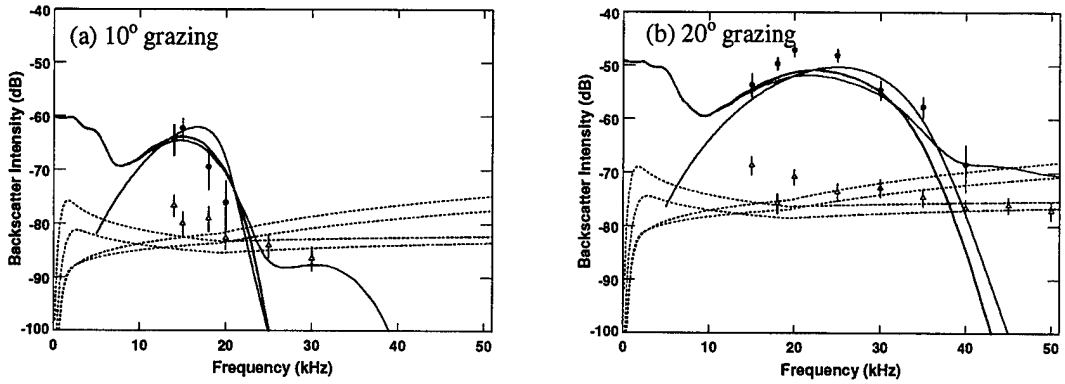

Fig. 7. Target and surface backscatter intensities for an oil-filled shell buried 5 cm below the mean height of a sinusoidal surface of 75-cm wavelength and 1.7-cm RMS height. The shell is located under a crest.

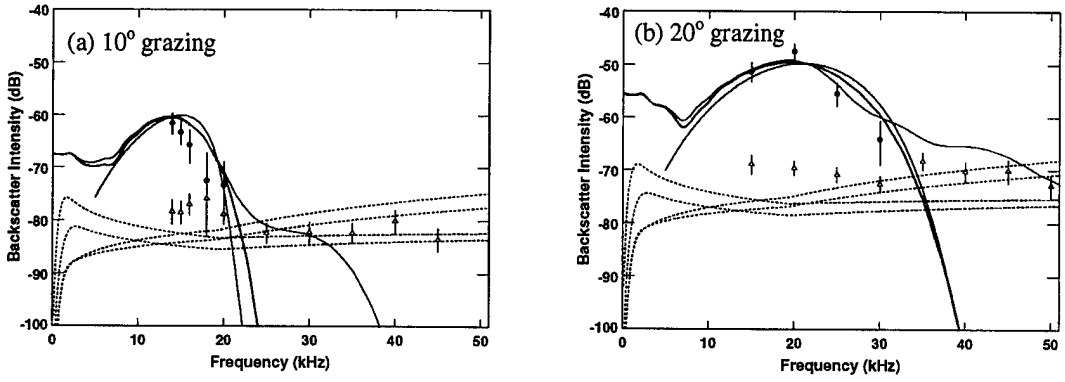

Fig. 8. Target and surface backscatter intensities for an oil-filled shell buried 17 cm below the mean height of a sinusoidal surface of 75-cm wavelength and 2.5-cm RMS height. The shell is located under a trough.

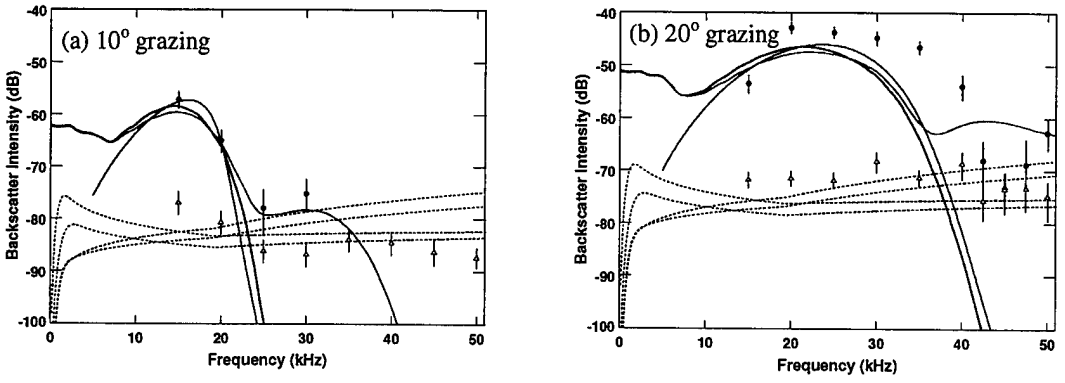

Fig. 9. Target and surface backscatter intensities for an oil-filled shell buried 8.5 cm below the mean height of a sinusoidal surface of 75-cm wavelength and 2.5-cm RMS height. The shell is located under a crest.

model in Figs. 7-9. Each of these models uses Rayleigh-Rice perturbation theory on the roughness to account for signal modifications caused by transmission across or scattering from the rough interface. All levels have been normalized to an incident RMS pressure of 1 μPa .

In all figures, four dotted curves correspond to reverberant noise level estimates based on the four sets of small-scale roughness parameters (Table 1) deduced from the IMP2 measurements. We include noise level estimates for all four sets of small-scale roughness measurements as a means of

obtaining a more robust noise estimate. This is motivated by two factors. First, the small-scale roughness was measured by IMP2 along a single 1-D track, while a measurement over a 2-D region would be needed to fully characterize the small-scale roughness. Second, there is no apparent basis for assuming that small-scale roughness would be created during ripple formation with statistical uniformity over the ripple patch, while extrapolation of roughness measurements from 1-D to 2-D implicitly assumes such uniformity. Also, while biological processes under natural conditions at sea may bring the small-scale roughness close to statistical uniformity, such processes are nearly absent in the test pond environment. The set of four small-scale roughness measurements provides at least some measure of the range of roughness that can be expected within the ripple patch.

The reverberant noise level estimates are obtained by using the parameters in Table 1 in a first-order-perturbation, ensemble-averaged, roughness model for the scattered intensity.[7] The model results assume a plane wave with an RMS amplitude of 1 μPa scatters from small-scale, power-law roughness. The overall level of the curves depends on the area of the effective (SAS-processed) bottom patch contributing to the detected reverberation. This area is given by the product of the range and cross-range resolutions. For the 0.2 ms source pulse incident on the bottom at 10° and 20° grazing angles, the range resolution was 22 cm and 23 cm, respectively. The cross-range resolution, *CRR*, was determined at each frequency according to[6, 8]

$$CRR = 1.46\,\mathrm{Max}[d/2, \lambda, R\lambda/2L], \qquad (3)$$

where d is the physical source aperture (15.2 cm), R is the slant range to the target (11.4 m), □is the acoustic wavelength, and L is the synthesized array length (5.2 m). An extra factor of 1.46 is included in this expression to account for the use of a Hamming window to reduce side lobes around image features. The resulting curves represent a range of variation that can be expected in reverberant noise level as a function of acoustic frequency. For comparison with these ensemble-averaged estimates, calibrated and spatially averaged reverberation levels seen in the SAS image data are represented by the open triangles. The error range for these data points is indicated by vertical bars and is based on the sum of (a) the statistical uncertainty in our estimate of the mean reverberation intensity and (b) our estimate for the uncertainty in transducer calibration. The statistical uncertainty is taken to be $\pm\sigma/\sqrt{N}$, where σ is the standard deviation of reverberation intensity, and N is the number of independent SAS resolution cells in the 2 m × 0.5 m region used to obtain the mean background noise level. The uncertainty in transducer calibration was estimated to be ±0.7 dB.

The spatially averaged noise levels in all figures appear in reasonable agreement with the ensemble-averaged predictions. Nevertheless, spatially averaged levels can be expected to exhibit moderate to high variability as a function of frequency and grazing angle. Shallow grazing angles require averaging to be done over a spatial swath that is limited in area due to nonuniform illumination of the bottom in range. This can lead to a poor average. Furthermore, at the low-frequency end of measurements, expanding sonar beams lead to contamination of the bottom reverberant noise with reflections off the pool surface. Therefore, bottom reverberation levels are not ideal as references for validating target signal level predictions as done in [2]; i.e., by comparing measured and predicted SNRs. However, they do provide an estimate for the range of SNR that can be expected in target backscatter measurements and are shown for this purpose.

Comparisons between measurements and target scattering models that include ripple-diffraction effects are made in Figs. 7-9 by the three solid curves and the filled circles; the latter representing properly calibrated peak target amplitudes in SAS-processed image spaces like those shown in Figs. 4 and 5. The error range for these data points is indicated by vertical bars and is again based on the sum of two terms: (a) the uncertainty in the apparent target level owing to the possibility of background reverberation adding or subtracting from the true target level and (b) our estimate for the uncertainty in transducer calibration (±0.7 dB). The uncertainty bounds introduced by reverberation are estimated by $20\log[(|p_t| \pm |p_r|)/p_0]$, where the measured target level (actually target plus reverberation) is $20\log(|p_t|/p_0)$, where $p_0 =$ 1 μPa, and where the mean (intensity averaged) reverberation level is $20\log(|p_r|/p_0)$. The solid black line corresponds to a simple sonar equation model (to be referred to as the SEM) that uses Eq. (14) in [1] to calculate the penetration, taking into account the measured ripple profile and the target strength estimate for the buried sphere. This model does not include penetration and scattering effects attributable to evanescent waves and would not be expected to be valid much below 10 kHz. The solid blue line corresponds to a model (to be referred to as the TM1) that uses the first-order penetrating field to calculate target scattering via a T-matrix formalism[9] adapted to account for the specified sinusoidal bottom roughness. The TM1 is a frequency-domain scattering model that assumes an incident pressure at the bottom normalized to an RMS amplitude of 1 μPa. To facilitate comparisons with measurements, the predictions of this model were smoothed. A sliding average on the backscatter amplitude was performed in the frequency domain using a 10 kHz window with shading and normalization determined by the frequency components associated with a 0.2 ms, window-centered sine wave pulse. This smoothing makes comparisons with the measured data points more realistic since averaging over the experimental pulse bandwidth is implicit in the SAS processing of the peak target amplitudes. Notably, the TM1 does account for scattering effects attributable to evanescent waves, which leads to the departure from the SEM below 10 kHz. Finally, the solid red line corresponds to an improved version of TM1 (to be referred to as the TM2) that uses the penetrating field to second-order in perturbation theory to calculate smoothed

target scattering levels. This gives rise to a departure of the predicted signal levels from those of the SEM and TM1 at higher frequencies.

Considering the complexity of the scattering problem, for most of the cases considered in Figs. 7-9, agreement between the various models and measurements is good. The basic trends predicted as a function of incident grazing angle, target burial depth, and ripple height appear to be followed well in Figs. 7, 8, and 9(a). The second-order refinements in the TM2 appear to produce slightly better agreement with the data at the upper frequency range of Figs. 7(b) and 8(b) and significantly better agreement in Fig. 9(a). Nevertheless, first-order perturbation theory captures most of the relevant trends in target scattering level in these cases, when the scattering level lies above the reverberation level, even at a fairly high ripple height (2.5 cm RMS). These results provide substantial confirmation of the ripple scattering mechanism for enhanced detection of buried targets using sonar at subcritical grazing angles.

The clear exception to the good agreement is the comparison in Fig. 9(b). A mismatch is observed beginning at around 25 kHz that is believed to be due to the inadequacy of second-order perturbation theory as developed in TM2. For this case, the perturbation parameter (the product of the wavenumber and the RMS height) at 20 kHz is already 2.1, high enough to cause concern for low-order perturbation theory. Interestingly, this is not seen to be a significant problem in Fig. 9(a) for a shallower grazing angle or in Fig. 8(b) for the same grazing angle and ripple height but a deeper target burial depth and target placement near a trough of the ripple rather than a crest.

In the model curves in Figs. 7-9, the SAS resolution cell size has been used to determine the surface patch size that contributes to the reverberation level. Effects of SAS resolution have not been included in modeling the buried target level; that is, the incident field has been taken as a plane wave and the SAS spatial resolution has not been invoked to limit the region on the surface that contributes to the target signal via surface scattering. This is in contrast to the approach we have used in previous work.[2,10] In that work we presented data for and modeled the relative levels of the target and the background reverberation. Using CW simulations we found that the target level would be reduced by the small size of the SAS resolution cell, because the patch size on the surface that scatters the target signal to the receiver is larger than the resolution cell size. Thus, if the SAS resolution were used to model the reverberation level, we argued that the target level would need to be reduced to compensate for the small size of the scattering patch. Since we were only interested in the relative levels of the target and reverberation, we chose to leave the target level unmodified and increase the surface area of the scattering patch contributing to the reverberation in such a way that the relative levels would be in accord with the implications drawn from the CW simulations.

We now believe, based on time domain considerations, that this adjustment in relative levels was unnecessary. For the present work the SAS resolution cell is smaller than the region on the surface contributing to the target return only in the down-range direction. The down-range spatial resolution for scattering from the sediment is set by the temporal resolution of the pulse. What matters for the target return is whether the dominant contributions that reach the receiver fall within the resolution time window. This turns out to be true even for paths that scatter from points outside the reverberation range resolution window on the surface. As a consequence, the effective range resolution window for the target return is greater than for the reverberation, and SAS resolution effects can be ignored for the target return. We intend in future work to revisit the analyses described in [2, 10] to examine how this change in understanding affects those results.

IV. SUMMARY

Further controlled measurements were presented here that continue a previous investigation[2] to demonstrate and validate a mechanism for shallow grazing angle acoustic detection of targets buried in sand having a sinusoidal, rippled sediment-water interface. For 50 and 75-cm wavelength ripple, 10° and 20° incident grazing angles (well below the critical angle of the sand), three target burial depths, and two ripple heights, a buried, silicone-oil-filled sphere was clearly detected and calibrated signal levels determined as a function of frequency.

Since the previously reported measurements, the scattering data with the 50-cm wavelength ripple was further analyzed to explain the range shift in the SAS-processed images of the buried sphere as a function of frequency. It was found that the range shift could be explained as a consequence of a frequency-dependent shift in the surface patch that contributes to the illumination of the target. Predictions for this shift are shown to be consistent with a first-order-perturbation diffraction law.

Calibrated signal levels from the 75-cm wavelength ripple measurements were compared to three acoustic scattering models that incorporate diffraction effects into the bottom by the sinusoidal sand ripples. Most of the data-model comparisons exhibited good agreement in the trends across the experimental bandwidth, even when compared against models based on first-order perturbation theory only. These results confirm that ripple diffraction is a valid mechanism for enhancing the detection of buried targets at shallow sonar grazing angles. However, exceptions to this agreement with low-order perturbation theory appear when the ripple amplitude is high.

ACKNOWLEDGMENTS

The authors gratefully acknowledge support from the

Office of Naval Research (ONR Codes 32OMCM, 321OE, and 321OA) and the Unexploded Ordnance Office of the Strategic Environmental Research and Development Program (SERDP) for this work. The authors also wish to thank the following for their participation and help in this effort: Ed Kloess, Jose Fernandez, and Dan Cook of the Coastal Systems Station; Vern Miller, Paul Aguilar, and Eric Boget of the Applied Physics Laboratory, University of Washington.

REFERENCES

[1] D. R. Jackson, K. L. Williams, E. I. Thorsos, and S. G. Kargl, "High-frequency subcritical acoustic penetration into a sandy sediment," *IEEE J. Ocean. Eng.*, **27**, 346-361 (2002)..

[2] J. L. Lopes, C. L. Nesbitt, R. Lim, D. Tang, K. L. Williams, and E. I. Thorsos, "Shallow grazing angle sonar detection of targets buried under a rippled sand interface" *Proceedings of Oceans 2002*, Biloxi, MS, Oct 28-Nov 1, 2002.

[3] D. Tang, K. B. Briggs, K. L. Williams, D. R. Jackson, and E. I. Thorsos, "Fine-scale volume heterogeneity measurements in sand," *IEEE J. Ocean. Eng.*, **27**, 546-560 (2002)..

[4] K. L. Williams, D. R. Jackson, E. I. Thorsos, and D. Tang, "Comparison of sound speed and attenuation measured in a sandy sediment to predictions based on the Biot theory of porous media," *IEEE J. Ocean. Eng.*, **27**, 413-428 (2002).

[5] K. B. Briggs, D. Tang, and K. L. Williams, "Characterization of interface roughness of rippled sand off Fort Walton Beach, Florida," *IEEE J. Ocean. Eng.*, **27**, 505-514 (2002).

[6] D. E. Hawkins, *Synthetic Aperture Imaging Algorithms: with Application to Wide Bandwidth Sonar*, Ph.D. Dissertation, University of Canterbury, Christchurch, New Zealand, October 1996.

[7] J. E. Moe and D. R. Jackson, "Near-field scattering through and from a 2-D fluid-fluid rough interface," *J. Acoust. Soc. Am.* **103**, 275-287 (1998).

[8] C. V. Jakowatz, Jr., D. E. Wahl, P. H. Eichel, D. C. Ghiglia, and P. A. Thompson, *Spotlight-Mode Synthetic Aperture Radar: A Signal Processing Approach* (Kluwer Academic Publishers, Boston, MA, 1999).

[9] R. Lim, K. L. Williams, and E. I. Thorsos, "Acoustic scattering by a three-dimensional elastic object near a rough surface," *J. Acoust. Soc. Am.*, **107**, 1246-1262 (2000).

[10] J. E. Piper, K. W. Commander, E. I. Thorsos, and K. L. Williams, "Detection of buried targets using a synthetic aperture sonar," IEEE J. Ocean. Eng., 27, 495-504 (2002).